crystals

MDPI

Article

Halogen Bonding in New Dichloride-Cobalt(II) Complex with Iodo Substituted Chalcone Ligands

Lukáš Masaryk [1], Ján Moncol [2], Radovan Herchel [1,*] and Ivan Nemec [1,3,*]

1 Department of Inorganic Chemistry, Faculty of Science, Palacký University, 17. listopadu 12, 771 46 Olomouc, Czech Republic; lukas.masaryk01@upol.cz
2 Department of Inorganic Chemistry, Faculty of Chemical and Food Technology, Slovak University of Technology in Bratislava, SK-81237 Bratislava, Slovakia; jan.moncol@stuba.sk
3 Central European Institute of Technology, Brno University of Technology, Purkyňova 123, 61200 Brno, Czech Republic
* Correspondence: radovan.herchel@upol.cz (R.H.); ivan.nemec@upol.cz (I.N.); Tel.: +420-58563-4435 (R.H.); +420-58563-4354 (I.N.)

Received: 7 April 2020; Accepted: 28 April 2020; Published: 30 April 2020

Abstract: The synthesis and properties of new chalcone ligand 4I-L ((2E)-1-[4-(1H-imidazol-1-yl)phenyl]-3-(4-iodophenyl)prop-2-en-1-one) and tetracoordinate Co(II) complex $[Co(4I\text{-}L)_2Cl_2]$, (1a), are reported in this article. Upon recrystallization of 1a, the single crystals of $[Co(4I\text{-}L)_4Cl_2]\cdot 2DMF\cdot 3Et_2O$ (1b) were obtained and crystal structure was determined using X-ray diffraction. The non-covalent interactions in 1b were thoroughly analyzed and special attention was dedicated to interactions formed by the peripheral iodine substituents. The density functional theory (DFT), atoms in molecule (AIM) and noncovalent interaction (NCI) methods and electronic localization function (ELF) calculations were used to investigate halogen bond formed between the iodine functional groups and co-crystallized molecules of diethyl ether.

Keywords: dichloride cobalt complex; chalcone; halogen bonding; Hirshfeld surfaces

1. Introduction

In molecular crystals, the building blocks, molecules, are held together by various directional and non-directional non-covalent intermolecular interactions. Some of these interactions have been widely explored, such as hydrogen bonding, cation/anion···π or π ···π interactions [1–5], but non-conventional interactions such as tetrel [6], pnictogen [7], chalcogen [8] and halogen bonding [9,10] have been less extensively studied [11,12]. All the above-mentioned interactions can be used to control the supramolecular architectures [13] of the coordination compounds and thus to influence their, e.g., mechanical [14], optical [15], catalytic [16], photochemical [17], luminescent [18] and magnetic properties [19]. In our recent research we devoted a lot of attention to prominence of non-covalent interactions in properties of magnetically bistable materials. We studied magnetic exchange interactions mediated by hydrogen bonding [20], π ···π interactions [21] or their combination [22]. We also discovered a new type of magnetic exchange pathway engaging Co···π interactions [23] and revealed possible influence of hydrogen bonding on occurrence of spin-crossover phenomenon [24]. In this report we focused our attention on interplay between halogen bonding and structure of mononuclear Co(II) coordination compounds, despite being aware of unpredictable competitiveness of hydrogen and halogen bonding [25]. These have a great potential to behave as molecular nanomagnets, so-called Single Ion Magnets (SIMs), due to large magnetic anisotropy exhibited by their central atoms in various symmetries of the ligand fields [26]. An inevitable condition for preparation of SIMs exhibiting high blocking temperatures in a zero-external magnetic field is the axial type of magnetic anisotropy

possessed by their metal centers. This can be achieved by careful choice of coordination number and polyhedral symmetry. It is well established that, for Co(II) compounds, very interesting results can be achieved for tetracoordinate coordination compounds exhibiting large distortion from ideal tetrahedral geometry [27]. To achieve significant distortions of coordination geometry, one can assume two viable strategies: (a) use of polydentate and sufficiently rigid ligands, (b) use of monodentate bulky ligands. Both strategies exploit steric hindrance of the ligands, which in (a) may be further supported by predefined bite angles of the chelating ligands [28]. In this work we explored approach (b) by using bulky monodentate ligands derived from chalcones of 4′-(imidazol-1-yl)acetophenone containing peripheral groups allowing formation of non-covalent interactions such as hydrogen or halogen bonding [29,30]. Such interactions can either induce or stabilize distortions of molecular shapes [31] or coordination polyhedrons [32,33]. Here, we report on the first results obtained using the above-mentioned approach. We used ligand 4I-L ((2E)-1-[4-(1H-imidazol-1-yl)phenyl]-3-(4-iodophenyl)prop-2-en-1-one) prepared by the aldol condensation [34] in reaction with $CoCl_2$ to obtain tetracoordinate complex $[Co(4I\text{-}L)_2Cl_2]$ in the powder form, (1a). Following recrystallization of 1a led to isolation of hexacoordinate complex $[Co(4I\text{-}L)_4Cl_2]\cdot 2DMF\cdot 3Et_2O$ (1b), (Et_2O stands for diethylether), the crystal structure of which was determined using single-crystal X-ray diffraction. The crystal structure of 1b contains rather weak non-covalent interactions, which were analyzed by calculating Hirshfeld surfaces and special attention was given to interactions provided by the peripheral iodine substituents. The O···I halogen bond formed by co-crystallized molecule of Et_2O was thoroughly studied by modern theoretical calculations, because reports on O···I halogen bonding involving Et_2O [35] or similar alkoxy compounds [36–41] are rare. Similarly, the crystal structures with short O···Cl (e.g., [42,43]) and O···Br (e.g., [44,45]) non-covalent interactions formed between halogen atoms and Et_2O molecules can be found in the Cambridge Structural Database (CSD version 2.0.4, [46]), but to the best of our knowledge, reports applying advanced theoretical calculations for better understanding the nature of this certain type of halogen bond are missing.

2. Experimental

2.1. Materials

$CoCl_2\cdot 6H_2O$ was purchased from Precious Metals Online, while other chemicals 4-iodobenzaldehyde, 4′-(imidazol-1-yl)acetophenone, NaOH, solvents (MeOH, diethyl ether (Et_2O), EtOH, dimethylformamide (DMF) and dichloromethane (DCM)) and deuterated solvents for NMR experiments (DMSO-d_6) were supplied by VWR International (Stříbrná Skalice, Czech Republic), Sigma-Aldrich (Prague, Czech Republic), Lach-Ner (Neratovice, Czech Republic) and Litolab (Chudobín, Czech Republic).

2.2. General Methods

Elemental analysis was performed by Flash 2000 CHNS Elemental Analyzer (Thermo Scientific, Waltham, MA, USA). Electrospray ionization mass spectrometry (ESI-MS; methanol solutions) was carried out with LCQ Fleet ion trap spectrometer (Thermo Scientific, Waltham, MA, USA; QualBrowser software, version 2.0.7) in both positive (ESI +) and negative (ESI-) ionization modes. ^1H and ^{13}C NMR spectroscopy, and ^1H-^{13}C gsHMQC and ^1H-^{13}C gsHMBC two dimensional correlation experiments were performed using DMSO-d_6 (HA1) solution at 300 K using Varian spectrometer (Palo Alto, CA, USA) at 400.00 MHz (for ^1H NMR) and 101.00 MHz (for ^{13}C NMR); gs = gradient selected, HMQC = heteronuclear multiple quantum coherence, HMBC = heteronuclear multiple bond coherence. ^1H and ^{13}C NMR spectra were calibrated against the residual DMF ^1H NMR (8.03, 2.92 and 2.75 ppm) and ^{13}C NMR (163.2, 34.9 and 29.8 ppm) signals. The splitting of proton resonances in the reported ^1H spectra is defined as s = singlet, d = doublet, dd = doublet of doublets, sep = septet, m = multiplet and bs = broad signal.

A Jasco FT/IR-4700 spectrometer (Jasco, Easton, MD, USA) was used for the collection of the infrared (IR) spectra of the studied ligand and complexes in the range of 400–4000 cm^{-1} by using the attenuated total reflection (ATR) technique on a diamond plate. UV-VIS spectroscopy was performed using a Perkin-Elmer (Waltham, MA, USA) Lambda 35 spectrometer at 11,000–40,000 cm^{-1}.

2.3. Crystal Structure Determination

Data collection and cell refinement of 1b were made by Stoe StadiVari (Stoe *& Cie* GmbH, Darmstadt, Germany) diffractometer using Pilatus3R 300K detector and microfocused X-ray source Incoatec IμS 2.0 HB (Ag *Kα* radiation). The structure was solved using SHELXT [47] program and refined by the full matrix least-squares procedure with Olex2.refine [48] in OLEX2 (version 1.3) [49]. The multi-scan absorption corrections were applied using the program Stoe LANA software [50]. The molecular structures and packing diagram were drawn with MERCURY [51]. Crystal Data for $C_{90}H_{96}Cl_2CoI_4N_{10}O_9$ (M = 2099.19 g/mol): triclinic, space group $P\bar{1}$ (no. 2), a = 8.5546(2) Å, b = 15.2289(3) Å, c = 18.6054(4) Å, α = 110.729(2)°, β = 90.916(2)°, γ = 102.814(2)°, V = 2198.59(9) $Å^3$, Z = 1, T = 100(1) K, μ(AgKα) = 0.915 mm^{-1}, D_{calc} = 1.585 g/cm^3, 61909 reflections measured (2.110° ≤ 2Θ ≤ 19.501°), 7765 unique (R_{int} = 0.0160) which were used in all calculations. The final R1 was 0.0405 ($I > 2\sigma(I)$) and wR_2 was 0.1180 (all data). The highest peak: +1.03 (0.84 Å from I1), the deepest hole −0.98 (0.90 Å from I1). Crystal structure refinement: All non-hydrogen atoms were refined anisotropically. The hydrogen atoms were placed into the calculated positions and they were included into the riding-model approximation with U_{iso} = 1.2U_{eq}(C) or 1.5 U_{eq} (CH_3) and d(C−H) = 0.95–0.98 Å. Non-routine aspects of the refinement: one of the Et_2O molecules is disordered over two positions with the oxygen atom lying on an inversion center.

2.4. Theoretical Calculations

The ORCA 4.2.1 computational package was employed for the presented calculations [52]. All the computations were based on the molecular fragments derived from the X-ray data, where only the positions of the hydrogen atoms were optimized using Density Functional Theory (DFT) with ωB97X-D3BJ functional [53] comprising the atom-pairwise dispersion correction (D3BJ) [54,55] with Sapporo-TZP-2012 basis set for all atoms [56]. The calculations exploited the resolution of identity approximation with the auxiliary basis created by the AutoAux generation procedure [57] and the chain-of-spheres approximation to exact exchange (RIJCOSX) [58,59]. The integration grids were increased by setting Grid5 and Gridx5, and the convergence criteria were set to tight SCF (self-consistent field) in all calculations. Then, the interaction energies (E_{int}) were calculated also taking into the account the basis set superposition error (BSSE). The further analysis was done with Multiwfn program [60,61]. The calculation of Hirshfeld [62] and shape index [63] surfaces were performed using the program Crystal Explorer 3.1 [64].

2.5. Synthesis of (2E)-1-[4-(1H-imidazol-1-yl)phenyl]-3-(4-iodophenyl)prop-2-en-1-one (4I-L)

A methanolic sodium hydroxide solution (40%; 1.2 mL) was added dropwise to a mixture of 4-iodobenzaldehyde (2 mmol, 0.464 g), 4′-(imidazol-1-yl)acetophenone (2 mmol, 0.370 g) and methanol (5 mL) over a period of 30–40 minutes with continuous stirring at room temperature until completion of the reaction (as indicated by TLC). The precipitates were filtered and washed with cold methanol–water mixture (1:10). Finally, the product was recrystallized from methanol [33].

Yellowish solid. Yield: 90%. ^{1}H NMR (400 MHz, DMSO-d_6, 298 K, ppm) δ 8.42 (s, 1H, C2-H), 8.26 (d, J = 8.7 Hz, 2H, C17-H, C21-H), 7.99 (d, J = 15.7 Hz, 1H, C14-H), 7.88–7.80 (m, 5H, C5-H, C7-H, C11-H, C18-H, C20-H), 7.72–7.64 (m, 3H, C8-H, C10-H, C15-H), 7.12 (s, 1H, C4-H). ^{13}C NMR (101 MHz, DMSO-d_6, 298 K, ppm) δ 188.24 (C12), 143.51 (C15-H), 140.77 (C6), 138.20 (C18-H, C20-H), 136.22 (C2-H), 135.88 (C9), 134.69 (C16), 131.21 (C8-H, C10-H), 130.98 (C17-H, C21-H), 130.85 (C4-H), 123.05 (C14-H), 120.30 (C7-H, C11-H), 118.24 (C5-H), 98.14 (C19-H). ESI+MS (MeOH, m/z,): 401.17 (calc. 401.22; 100%; {4I-L+H}$^+$), 423.05 (calc. 401.20; 32%; {4I-L+Na}$^+$). IR (ATR, ν, cm^{-1}): 408w, 463w,

507w, 538w, 594w, 652w, 677w, 727w, 812s, 830m, 960w, 981w, 1031w, 1060w, 1118w, 1165m, 1215m, 1289m, 1337w, 1428w, 1492w, 1512m, 1588s, 1652s, 2150w, 3118w.

2.6. Complex [Co(4I-L)$_2$(Cl)$_2$] (1a)

The solution of $CoCl_2 \cdot 6H_2O$ (0.5 mmol, 0.119 g) in 5 mL of methanol was heated up to 50 °C and then 2 molar equiv. of 4I-L were added (2 mmol, 0.400 g). The solution was allowed to cool down and then the reaction mixture was stirred at ambient temperature for 2 hours. The obtained blue precipitate was collected by filtration and washed with water (2 × 0.5 mL) and Et_2O (2 × 1 mL). The blue solid product was dried in desiccator under reduced pressure (overnight). Compound 1b was prepared by recrystallization of 1a from DMF/CH_3OH solvent mixture by slow diffusion of Et_2O in closed flask. Only small amounts of light blue crystals of 1b was isolated and, therefore, no technique other than single-crystal diffraction was used for characterization of this compound.

Yield: 84%. Anal. Calcd. for $CoC_{36}H_{26}Cl_2N_4I_2O_2$ (1a): C, 46.48; H, 2.82; N, 6.02%; found: C, 46.41; H, 2.72; N, 5.86%. ESI+MS (MeOH, m/z,): 401,14 (calc. 401.22; 30%; {4I-L+H}$^+$), 567.09 (calc. 567.06; 100%; {[Co(4I-L)(Cl)$_2$]+2H$_2$O+H}$^+$), 894.02 (calc. 893.91; 66%; {[Co(4I-L)(Cl)$_2$]+2H$_2$O+H}$^+$). IR (ATR, v, cm^{-1}): 402w, 448w, 490w, 522w, 605w, 647w, 735w, 811s, 962w, 1002w, 1062w, 1119w, 1182w, 1213w, 1318m, 1395w, 1479w, 1519m, 1602s, 1657s, 2159w, 3131w.

3. Results and Discussion

3.1. Synthesis and Basic Characterizations

The chalcone ligand 4I-L was prepared by aldol condensation of 4'-(imidazol-1-yl)acetophenone with the 4-iodobenzaldehyd as is shown in Scheme 1. The purity and structure of 4I-L were confirmed by NMR spectroscopy and elemental analysis. The ^{1}H NMR (see ESI, Figure S1), ^{13}C NMR (see ESI, Figure S2), spectra of 4I-L in DMSO-d_6 showed shifts characteristic for the aromatic functional groups (the list of all observed peaks can be found in the experimental chapter). The representative peak confirming the presence of the olefinic moiety resulting from aldol condensation (C14-H) was observed in ^{1}H NMR spectra approximately at 7.99 ppm. In the ^{13}C NMR spectra corresponding peak of C14-H was observed approximately at 123.05 ppm. The C-H groups were assigned by ^{1}H-^{13}C HMQC correlation experiments (Figure 1 left), while quaternary carbon atoms were assigned by ^{1}H-^{13}C HMBC correlation experiments.

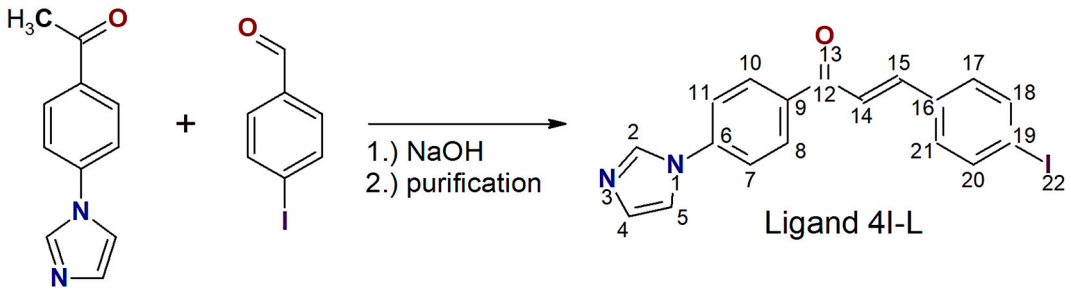

Scheme 1. Preparation of ligand 4I-L with given atom numbering scheme.

The complex 1a was prepared by reaction between $CoCl_2 \cdot 6H_2O$ and 4I-L (molar ratio 1:2) in methanolic solution as a blue precipitate. The elemental composition (CHN analysis) corresponds rather well with formula [Co(4I-L)$_2$Cl$_2$], and this assumption was further supported by the results of ESI+ mass spectroscopy, which revealed occurrence of peaks with suitable *m*/*z* isotopic distribution attributable to the {[Co(4I-L)$_2$(Cl)}$^+$ species (see ESI, Figure S3). The FTIR spectra showed valence vibration of the chalcone ketone group (ν(C=O)) at ca. 1600 cm^{-1}. The UV-VIS spectroscopy of 1a measured in the solid state showed absorption bands centered at ca. 600 nm (Figure 1 right), which can be attributed to spin allowed *d*-*d* transitions characteristic for the tetracoordinate Co(II) complexes [65].

The spectral band was fitted to three Gaussian primitives having peak maxima at 518 nm, 578 nm and 631 nm (Figure 1 right). The individual bands originate from $^4A_2 \rightarrow {}^4T_1(P)$ transition in ideal T_d symmetry [66], although the $^4T_1(P)$ term splits into three individual terms ($^4A_2(P)$, $^4B_1(P)$ and $^4B_2(P)$) in lower symmetry (expected symmetry of coordination polyhedron of 1a is C_{2v}). Thus, it may be concluded that compound 1a is tetracoordinate Co(II) complex with the formula $[Co(4I\text{-}L)_2Cl_2]$.

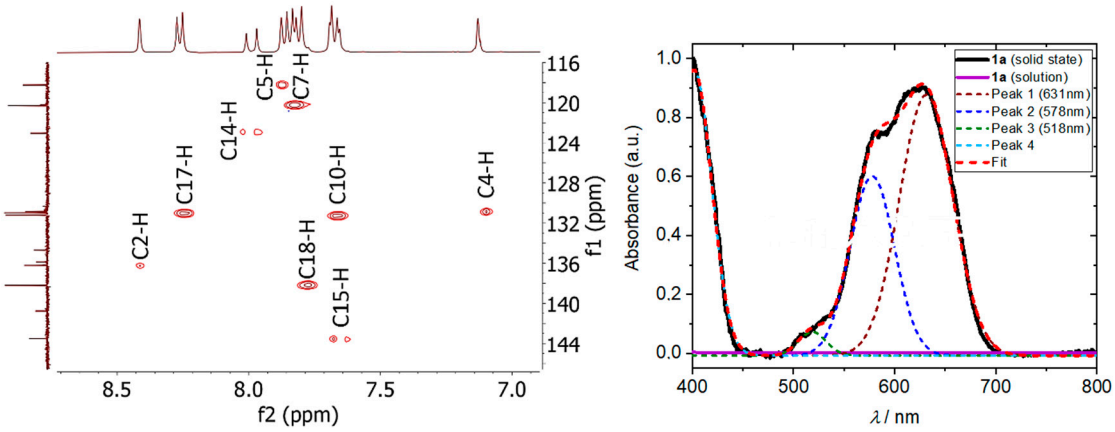

Figure 1. *Left*—HMCQ NMR spectrum of the ligand 4I-L; DMSO-d_6 solutions. See Scheme 1 for the structural formula and atom numbering scheme. *Right*—UV-VIS absorption spectrum measured for **1a** in the solid state (black line) and methanolic solution (violet line) in the range of 400–800 nm. Fit to four Gaussian primitives shown as dashed lines with peak maxima listed in the legend.

Complex 1a is only negligibly soluble in water, methanol, ethanol or acetone, but it is well soluble in DMF or DMSO. The UV-VIS spectrum measured for CH_3OH solution of 1a revealed no strong absorption bands in the range of 400–800 nm (Figure 1 right). Interestingly, upon recrystallization of 1a from CH_3OH/DMF solvent mixture, followed by slow diffusion of Et_2O, the small amount of light blue crystals precipitated. The selected single crystal was subjected to the X-ray diffraction analysis, which revealed that the prepared complex 1b is hexacoordinate (*vide infra*).

3.2. Crystal Structure

Compound 1b crystallizes in the triclinic crystal system with the space group $P\bar{1}$. The Co atom lies on a crystallographic inversion center (1h) and thus the asymmetric unit consists of the half of the complex molecule $[Co(4I\text{-}L)_4Cl_2]$, one DMF molecule and one and half Et_2O molecules, which altogether gives formula of $[Co(4I\text{-}L)_4Cl_2]\cdot 2DMF\cdot 3Et_2O$. The complex molecule is hexacoordinate and it consists of four 4I-L and two chlorido ligands coordinated to Co(II) center. The 4I-L ligands adopt *E*-configuration and coordinate the Co(II) atom by nitrogen donor atoms from the imidazolyl moieties forming equatorial plane with rather dissimilar Co−N bond lengths (d(Co−N) = 2.121(3) and 2.162(3) Å). The axial coordination sites are occupied by two chlorido ligands with rather long Co−Cl bonds (d(Co−Cl) = 2.4880(9) Å). The overall geometry of the coordination polyhedron can be described best as an axially elongated octahedron (Figure 2).

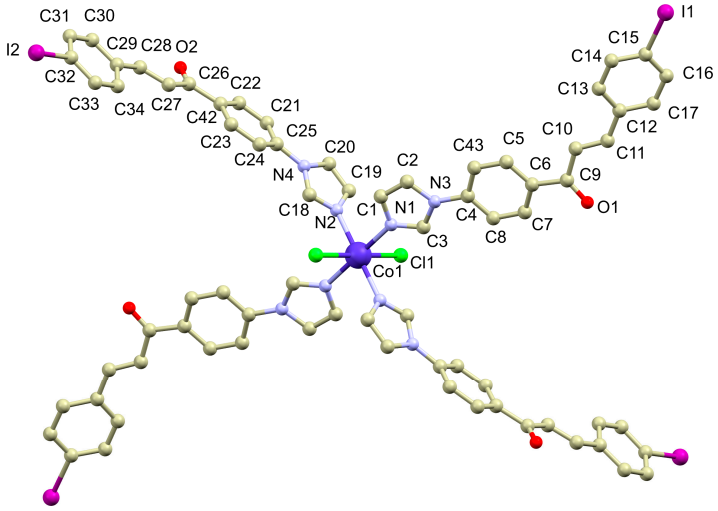

Figure 2. Molecular structure of 1b. Color code: grey (C), green (Cl), dark blue (Co), violet (I), light blue (N) and red (O). Hydrogen atoms are omitted for clarity. Selected bond lengths (in Å) and angles (deg.): *d*(Co1−N1) = 2.121(3), *d*(Co1−N2) = 2.162(3), *d*(Co1−Cl1) = 2.4880(9), N1−Co1−N1^{i} = N2−Co1−N2^{i} = Cl1−Co1−Cl1^{i} = 180.0, N1−Co1−N2 = 88.15(12), N1−Co1−Cl1 = 92.26(9), N1−Co1−Cl1^{i} 87.74(9), N2−Co1−Cl1^{i} = 90.14(9), N2−Co1−Cl1 = 89.86(9). Symmetry code: (i) =1 -x, 1 -y, 1 -z.

The complex molecules are stabilized in the structure by plethora of weak intermolecular contacts and therefore analysis of the Hirschfeld surface was performed to identify them (Figures S4 and S5, the parameters of hydrogen bonds are listed in Table S1). The complex molecules are organized in supramolecular chains by bifurcated C−H···Cl hydrogen bonding between the aromatic C−H groups located on 1-phenyl-imidazolyl fragment of the 4I-L ligand from adjacent complex molecule (*d*(C···Cl) = 3.466(5) and 3.673(5), Å Figure 3a). The chlorido ligand also acts as an acceptor of another C−H···Cl hydrogen bond involving C−H group from the DMF molecule (*d*(C···Cl) = 3.807(4) Å). Interestingly, the DMF molecule is further stabilized in the crystal structure by set of three rather strong C−H···O hydrogen bonds between three C−H groups from the 4I-L ligand and oxygen atom of the DMF molecule (*d*(C···O) = 3.324(6), 3.388(5) and 3.394(5) Å, Figure 3b).

One of the chalcone ligands forms offset π-π stacking interactions with the adjacent counterpart related by operation of inversion. The shortest C···C distances are rather short (*d*(C···C) = 3.290(5) and 3.357(5) Å, Figure 4a). These interactions can be visualized best by calculating Hirshfeld surface followed by highlighting areas corresponding to C···C interactions (Figure 4c). Furthermore, by inspecting the shape-index surfaces we were able to confirm these interactions because of appearance of neighboring red and blue triangular map areas (red circles), which are characteristic for occurrence of π-π stacking [67,68].Both types of the supramolecular dimers, (a) and (b), are extended to chain substructures due to the inversion symmetry. The keto oxygen atoms are involved in the weak C−H···O hydrogen bonds, where one of the keto groups forms a pair of bifurcated hydrogen bonds with the C−H groups of the benzyl-imidazolyl moiety (*d*(C···O) = 3.193(5) and 3.420(4) Å, Figure 4a). The second keto group forms only weak C−H···O non-covalent contacts.

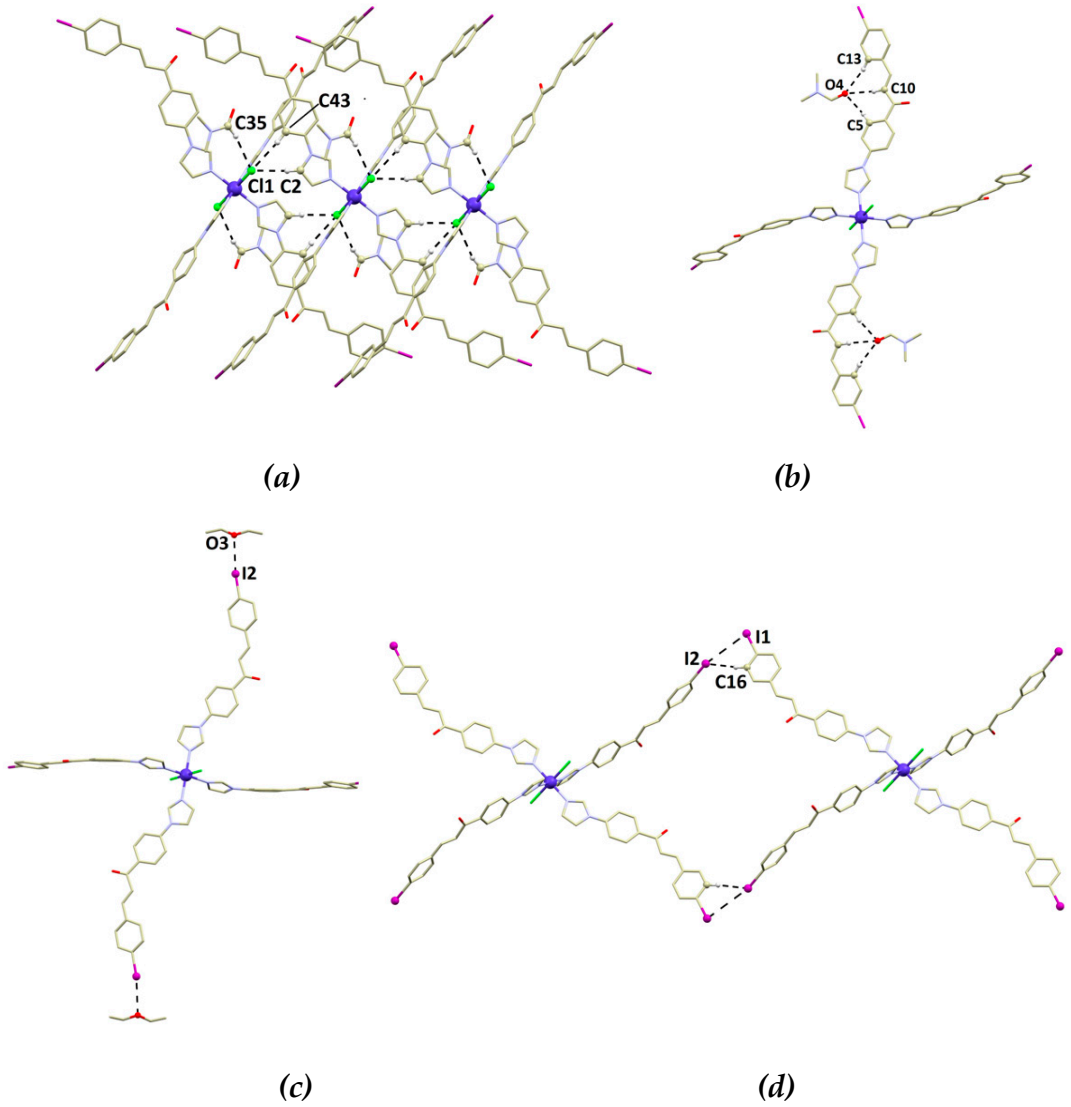

Figure 3. A perspective view on the non-covalent interactions in 1b. (***a***) Supramolecular chain formed by C−H···Cl hydrogen bonding: *d*(C2···Cl1) = 3.466(5) Å, *d*(C35···Cl1) = 3.807(4) Å, *d*(C43···Cl1) = 3.673(5) Å. (***b***) Bifurcated C−H···O hydrogen bonding of the DMF molecule: *d*(C5···O4) = 3.324(6) Å, *d*(C10···O4) = 3.388(5) Å, *d*(C13···O4) = 3.394(5) Å. A perspective view on the I···O halogen bonding (***c***) and C−H···I non-covalent interaction (***d***). Donor-acceptor distances of displayed interactions: *d*(I2···O3) =3.264(4) Å, *d*(C16···I2) = 3.918(4) Å, *d*(I1···I2) = 4.1676(5) Å. Hydrogen atoms (except for those involved in hydrogen bonding) were omitted for clarity. The non-covalent interactions were depicted as black dashed lines.

Two symmetry-independent iodine substituents on the 4I-L ligands form different types of the non-covalent interactions. One of them forms I···O type of the interaction, since it is capped by co-crystallized Et_2O molecule at rather short distance: *d*(I···O) = 3.264(4) Å (Figure 3c). The other one forms two weak contacts with two neighboring functional groups on the 4I-L ligand: one with the above-mentioned iodine substituent (*d*(I···I) = 4.1676(5) Å) and the second one with the neighboring C-H group (*d*(C···I) = 3.918(5) Å, Figure 3d).

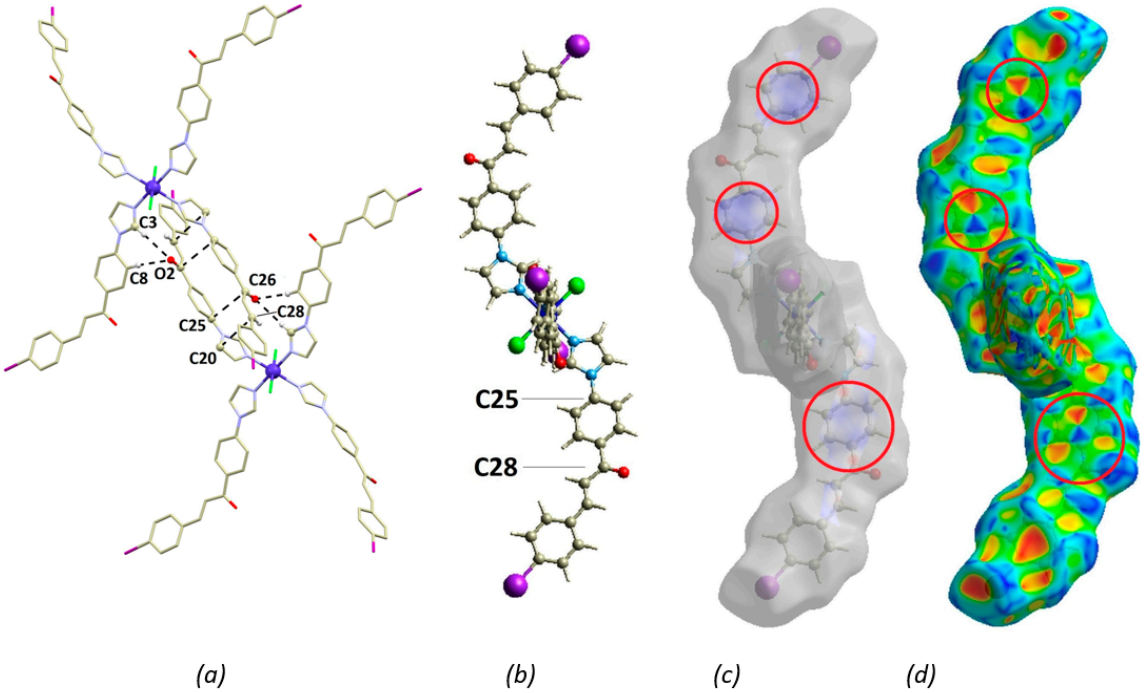

Figure 4. (***a***) A perspective view on π-π stacking interactions and bifurcated C−H···O hydrogen bonding involving chalcone keto group. Donor-acceptor distances of displayed interactions: *d*(C20···C28) = 3.357(5) Å, *d*(C25···C26) = 3.290(5) Å, *d*(C3···O2) = 3.421(6) Å, *d*(C8···O2) = 3.193(5) Å. The non-covalent interactions were depicted as black dashed lines. Hydrogen atoms (except for those involved in hydrogen bonding) were omitted for clarity. The drawing of molecular structure of 1b with the atom labels of the carbon atoms involved in short C···C contacts (***b***). Calculated Hirshfeld surfaces (d_{norm}) with highlighted areas of the C···C interactions (colored maps in red circles, ***c***) and shape-index surface with highlighted areas involved in π-π stacking interactions (red circles, ***d***).

3.3. Theoretical Studies

The DFT theory was employed together with ORCA program to evaluate the interaction energies for selected non-covalent contacts affecting the crystal packing with range-separated functional ωB97X-D3BJ. First, the I···O type of the interaction between 4I-L ligand and co-crystallized Et_2O molecule was dealt with (Figure 3c). Thus, for the molecular fragment {(4I-L)···(Et_2O)} shown in Figure 5, the computed interaction energy is E_{int} = −4.401 kcal/mol. Next, the I···I type of the interaction (Figure 3d) between two 4I-L ligands {(4I-L)···(4I-L)} from different complex moieties was inspected and the calculation resulted in E_{int} = −2.212 kcal/mol (Figure 5). Moreover, these interactions were analyzed with the noncovalent interaction (NCI) method [69] with the help of Multiwfn software. This method is based on the analysis of the electron density (ρ) by defining the reduced density gradient (RDG) function which helps to identify the weak intra/inter molecular interactions and the nature of these interactions, thus attractive vs repulsive, is analyzed by the sign of eigenvalue λ_2 of the electron density Hessian matrix. These interactions were successfully visualized with VMD program [70] as sign (λ_2)ρ values in Figure 5. It is evident that in {(4I-L)···(4I-L)} molecular fragment (Figure 5 *top*) two types of weak interactions are present, the hydrogen bond C−H···I and halogen bond I···I, whereas the second fragment {(4I-L)···(Et_2O)}, (Figure 5 *bottom*), is dominated by O···I halogen bond. Indeed, the topological analysis based on the atoms in molecules (AIM) method [71] implemented in Multiwfn program identified the bond critical points (BCP) of the type (3,−1) as depicted in Figure 6 together with the bond paths, which follow the maximal gradient path connecting two BCPs. Next, the NCI sign(λ_2)ρ values were calculated in selected BCPs as −0.00529 for I···I, −0.0103 for C-H···I and −0.0102 for O···I contacts.

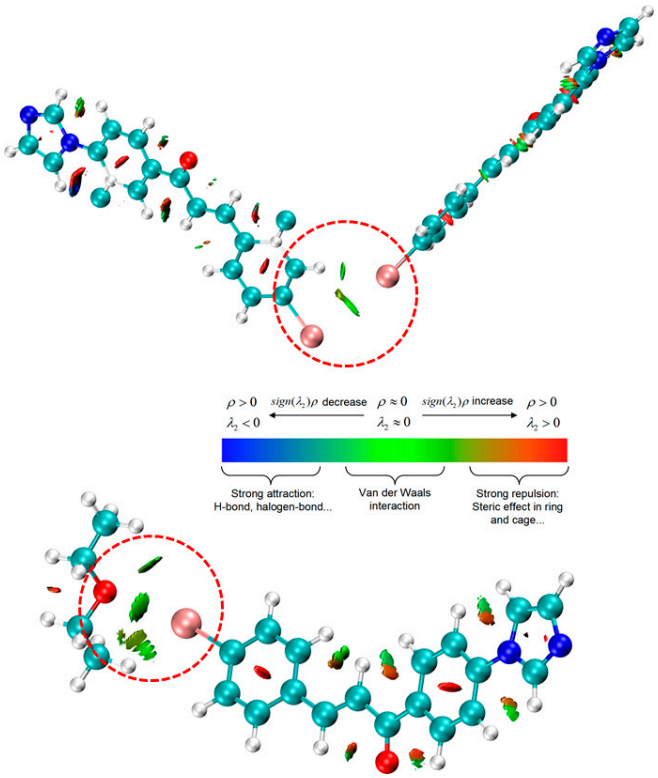

Figure 5. The molecular fragments {(4I-L)···(4I-L)} (*top*) and {(4I-L)···(Et_2O)} (*bottom*) used for the theoretical calculations of the interaction energies (E_{int}) overlapped with NCI calculations showing weak intermolecular interactions of interest in red dashed circles.

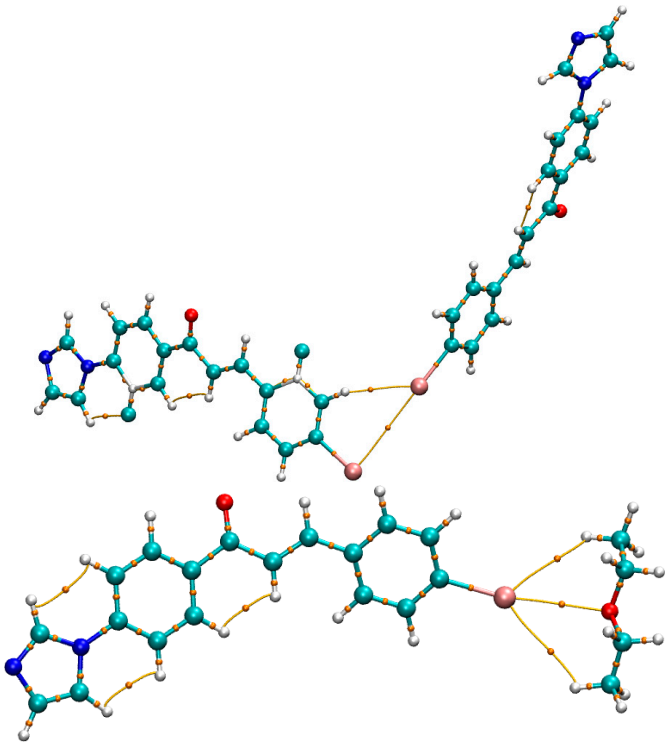

Figure 6. The molecular fragments {(4I-L)···(4I-L)} (*top*) and {(4I-L)···(Et_2O)} (*bottom*) showing the atoms in molecules (AIM) analysis indicating the position of the bond electron density critical points (BCP) of the type (3, −1) as small orange spheres together with calculated bond paths (yellow lines).

Thus, we can conclude that all these interactions are attractive and sort them by the increasing strength as I···I < C-H···I ≈ O···I, which agrees with the DFT calculated energies. It well known that halogen bonds are characteristic by formation of so-called σ-holes on heavy halogen atoms, which can interact with an electron pair of the electron donor atom. To better understand and visualize this phenomenon, Multiwfn package was used to calculate Electron Localization Function (ELF). The ELF was introduced by Becke and Edgecombe [72] and its application to the study of electronic structure is discussed by Lu and Chen [73]. Thus, the colored mapped figures were calculated as shown in Figure 7 to elucidate the distribution of electron density by ELF. Indeed, in both cases of I···I (Figure 7 *left*) and O···I (Figure 7 *right*) halogen bonds, the presence of σ-holes on I atoms is evident and the complementary donor electron pair of I or O atoms is present too. The detailed view of ELF along the particular AIM calculated bond paths (Figure 7) is also depicted in Figure S6.

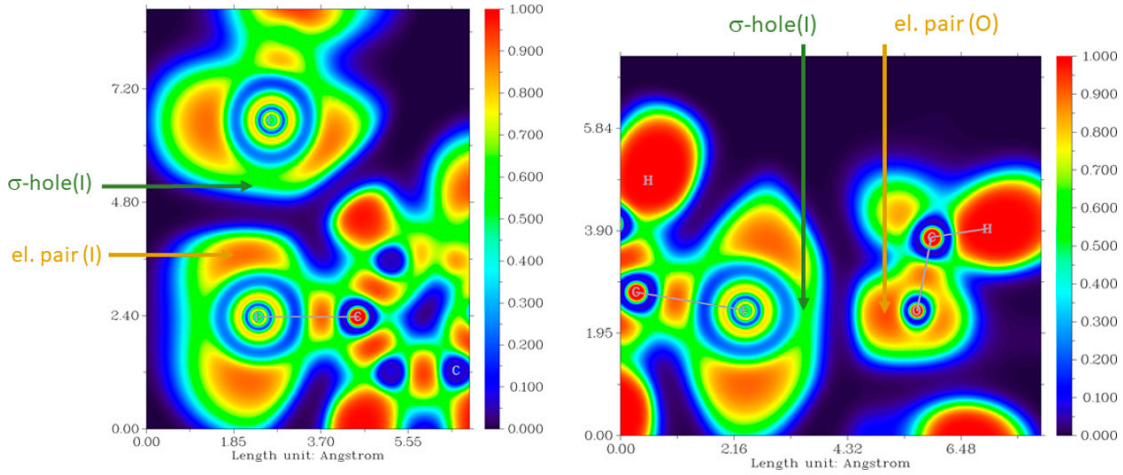

Figure 7. The calculated Electron localization function (ELF) for the molecular fragments {(4I-L)···(4I-L)} (***left***) and {(4I-L)···(Et_2O)} (***right***) showing halogen bonds of the types I···I and O···I.

4. Conclusions

In this article, we reported on the synthesis of the chalcone ligand (2E)-1-[4-(1H-imidazol-1-yl)phenyl]-3-(4-iodophenyl)prop-2-en-1-one (4I-L), which was further used for synthesis of tetracoordinate complex [Co(4I-L)Cl_2], (1a), which after recrystallization transformed into hexacoordinate complex [Co(4I-L)$_4Cl_2$]·2DMF·3Et_2O, (1b). Ligand and complex 1a were thoroughly characterized by spectroscopic techniques and for 1b, the crystal structure was determined by X-ray diffraction analysis. It was revealed that 1b is hexacoordinate Co(II) complex with chlorido ligands in the axial positions. The crystal structure of 1b is stabilized by a plethora of weak non-covalent interactions, mainly by C−H···O, C−H···Cl and $\pi-\pi$ stacking of aromatic rings. Furthermore, the peripheral iodine substituents on the 4I-L ligands form I···O, C−H···I and I···I non-covalent interactions. These were theoretically studied by the DFT, NCI, AIM and ELF calculations and all confirmed formation of halogen bond of significant strength in the case of the I···O contact. The weak nature of the C−H···I hydrogen bonding and I···I interaction was confirmed.

Supplementary Materials: The following are available online at http://www.mdpi.com/2073-4352/10/5/354/s1, Figure S1: ^{1}H NMR spectrum of ligand 4I-L in DMSO-d_6, Figure S2: ^{13}C NMR spectrum of ligand 4I-L in DMSO-d_6, Figure S3: ESI-MS mass spectrum of complex **1a** in methanol, Figure S4: 2D fingerprint plots generated for the complex molecule [Co(4I-L)$_4Cl_2$], Figure S5: Hirshfeld surface calculated for the complex molecule [Co(4I-L)$_4Cl_2$], Figure S6:The calculated Electron localization function (ELF) along calculated bond paths for the molecular fragments {(4I-L)···(4I-L)} (top) and {(4I-L)···(Et_2O)} (bottom) showing halogen bonds of the types I···I and O···I. The dotted line locates the BCP (3,-1, Table S1: summary of hydrogen bonding parameters.

Author Contributions: Conceptualization: L.M. and I.N.; Formal analysis: L.M., J.M., R.H., I.N.; Investigation: L.M., J.M.; Writing—original draft: I.N., R.H.; Writing—review & editing: L.M., J.M., I.N., R.H.; All authors have read and agreed to the published version of the manuscript.

Funding: This research was funded by Palacký University Olomouc (PrF_2020_016) and also supported by the Grant Agencies of the Slovak Republic, (VEGA 1/0639/18, APVV-18-0016) and MŠVVaŠ of the Slovak Republic within the Research and Development Operation Program for the project "University Science Park of STU Bratislava" (ITMS project no. 26240220084) cofounded by the European Regional Development Fund.

Conflicts of Interest: The authors declare no competing financial interests.

References

1. Jeffrey, G.A. Hydrogen-Bonding: An update. *Crystallogr. Rev.* **2003**, *9*, 135–176. [CrossRef]
2. Steiner, T. C–H···O hydrogen bonding in crystals. *Crystallogr. Rev.* **2003**, *9*, 177–228. [CrossRef]
3. Tiekink, E.R.T.; Zukerman-Schpector, J. Gold···π aryl interactions as supramolecular synthons. *CrystEngComm* **2009**, *11*, 1176. [CrossRef]
4. Chen, T.; Li, M.; Liu, J. π–π Stacking Interaction: A Nondestructive and Facile Means in Material Engineering for Bioapplications. *Cryst. Growth Des.* **2018**, *18*, 2765–2783. [CrossRef]
5. Watt, M.M.; Collins, M.S.; Johnson, D.W. Ion−π Interactions in Ligand Design for Anions and Main Group Cations. *Acc. Chem. Res.* **2012**, *46*, 955–966. [CrossRef]
6. Bauzá, A.; Seth, S.; Frontera, A. Tetrel bonding interactions at work: Impact on tin and lead coordination compounds. *Coord. Chem. Rev.* **2019**, *384*, 107–125. [CrossRef]
7. Alkorta, I.; Elguero, J.; Frontera, A. Not Only Hydrogen Bonds: Other Noncovalent Interactions. *Crystals* **2020**, *10*, 180. [CrossRef]
8. Gleiter, R.; Haberhauer, G.; Werz, D.B.; Rominger, F.; Bleiholder, C. From Noncovalent Chalcogen–Chalcogen Interactions to Supramolecular Aggregates: Experiments and Calculations. *Chem. Rev.* **2018**, *118*, 2010–2041. [CrossRef]
9. Cavallo, G.; Metrangolo, P.; Milani, R.; Pilati, T.; Priimagi, A.; Resnati, G.; Terraneo, G. The Halogen Bond. *Chem. Rev.* **2016**, *116*, 2478–2601. [CrossRef]
10. Kolář, M.H.; Hobza, P. Computer Modeling of Halogen Bonds and Other σ-Hole Interactions. *Chem. Rev.* **2016**, *116*, 5155–5187. [CrossRef]
11. Carreras, L.; Benet-Buchholz, J.; Franconetti, A.; Frontera, A.; Van Leeuwen, P.W.N.M.; Vidal-Ferran, A. Halogen bonding effects on the outcome of reactions at metal centres. *Chem. Commun.* **2019**, *55*, 2380–2383. [CrossRef] [PubMed]
12. Zhao, Y.; Cotelle, Y.; Sakai, N.; Matile, S. Unorthodox Interactions at Work. *J. Am. Chem. Soc.* **2016**, *138*, 4270–4277. [CrossRef] [PubMed]
13. Amabilino, D.B.; Smith, D.K.; Steed, J.W. Supramolecular materials. *Chem. Soc. Rev.* **2017**, *46*, 2404–2420. [CrossRef] [PubMed]
14. Chakrabarty, R.; Mukherjee, P.S.; Stang, P.J. Supramolecular Coordination: Self-Assembly of Finite Two- and Three-Dimensional Ensembles. *Chem. Rev.* **2011**, *111*, 6810–6918. [CrossRef]
15. El-Mellouhi, F.; Bentria, E.T.; Marzouk, A.; Rashkeev, S.N.; Kais, S.; Alharbi, F.H. Hydrogen bonding: A mechanism for tuning electronic and optical properties of hybrid organic–inorganic frameworks. *npj Comput. Mater.* **2016**, *2*, 16035. [CrossRef]
16. Raynal, M.; Ballester, P.; Vidal-Ferran, A.; Van Leeuwen, P.W.N.M. Supramolecular catalysis. Part 1: Non-covalent interactions as a tool for building and modifying homogeneous catalysts. *Chem. Soc. Rev.* **2014**, *43*, 1660–1733. [CrossRef]
17. Ramamurthy, V.; Sivaguru, J. Supramolecular Photochemistry as a Potential Synthetic Tool: Photocycloaddition. *Chem. Rev.* **2016**, *116*, 9914–9993. [CrossRef]
18. Mako, T.; Racicot, J.M.; Levine, M. Supramolecular Luminescent Sensors. *Chem. Rev.* **2018**, *119*, 322–477. [CrossRef]
19. Kahn, O. *Magnetism: A Supramolecular Function*; Springer: Dordrecht, The Netherlands, 1996; ISBN 978-94-015-8707-5.
20. Nemec, I.; Herchel, R.; Šilha, T.; Trávníček, Z. Towards a better understanding of magnetic exchange mediated by hydrogen bonds in Mn(III)/Fe(III) salen-type supramolecular dimers. *Dalton Trans.* **2014**, *43*, 15602–15616. [CrossRef]

21. Nemec, I.; Herchel, R.; Šalitroš, I.; Travnicek, Z.; Moncol, J.; Fuess, H.; Ruben, M.; Linert, W. Anion driven modulation of magnetic intermolecular interactions and spin crossover properties in an isomorphous series of mononuclear iron(iii) complexes with a hexadentate Schiff base ligand. *CrystEngComm* **2012**, *14*, 7015. [CrossRef]
22. Herchel, R.; Nemec, I.; Machata, M.; Travnicek, Z. Experimental and Theoretical Investigations of Magnetic Exchange Pathways in Structurally Diverse Iron(III) Schiff-Base Complexes. *Inorg. Chem.* **2015**, *54*, 8625–8638. [CrossRef] [PubMed]
23. Nemec, I.; Herchel, R.; Travnicek, Z. Ferromagnetic coupling mediated by Co···π non-covalent contacts in a pentacoordinate Co(ii) compound showing field-induced slow relaxation of magnetization. *Dalton Trans.* **2016**, *45*, 12479–12482. [CrossRef]
24. Nemec, I.; Herchel, R.; Travnicek, Z. The relationship between the strength of hydrogen bonding and spin crossover behaviour in a series of iron(iii) Schiff base complexes. *Dalton Trans.* **2015**, *44*, 4474–4484. [CrossRef] [PubMed]
25. Awwadi, F.F.; Taher, D.; Haddad, S.F.; Turnbull, M.M. Competition between Hydrogen and Halogen Bonding Interactions: Theoretical and Crystallographic Studies. *Cryst. Growth Des.* **2014**, *14*, 1961–1971. [CrossRef]
26. Gómez-Coca, S.; Aravena, D.; Morales, R.; Ruiz, E. Large magnetic anisotropy in mononuclear metal complexes. *Coord. Chem. Rev.* **2015**, *289*, 379–392. [CrossRef]
27. Nemec, I.; Herchel, R.; Kern, M.; Neugebauer, P.; Van Slageren, J.; Travnicek, Z. Magnetic Anisotropy and Field-induced Slow Relaxation of Magnetization in Tetracoordinate Co^{II} Compound $[Co(CH_3\text{-im})_2Cl_2]$. *Materials* **2017**, *10*, 249. [CrossRef]
28. Alvarez, S. Distortion Pathways of Transition Metal Coordination Polyhedra Induced by Chelating Topology. *Chem. Rev.* **2015**, *115*, 13447–13483. [CrossRef]
29. Siskos, M.G.; Choudhary, M.I.; Gerothanassis, I.P. Hydrogen Atomic Positions of O–H···O Hydrogen Bonds in Solution and in the Solid State: The Synergy of Quantum Chemical Calculations with 1H-NMR Chemical Shifts and X-ray Diffraction Methods. *Molecules* **2017**, *22*, 415. [CrossRef]
30. Sobczyk, L.; Chudoba, D.; Tolstoy, P.M.; Filarowski, A. Some Brief Notes on Theoretical and Experimental Investigations of Intramolecular Hydrogen Bonding. *Molecules* **2016**, *21*, 1657. [CrossRef]
31. Sen, S.; Kaseman, D.C.; Colas, B.; Jacob, D.; Clark, S. Hydrogen bonding induced distortion of CO 3 units and kinetic stabilization of amorphous calcium carbonate: Results from 2D 13 C NMR spectroscopy. *Phys. Chem. Chem. Phys.* **2016**, *18*, 20330–20337. [CrossRef]
32. Fielden, J.; Long, D.L.; Speldrich, M.; Kögerler, P.; Cronin, L. $[Co_xCu_{1-x}(DDOP)(OH_2)(NO_3)](NO_3)$: Hydrogen bond-driven distortion of cobalt(ii) by solid solution 'network mismatch'. *Dalton Trans.* **2012**, *41*, 4927. [CrossRef] [PubMed]
33. Dahl, E.W.; Szymczak, N.K. Hydrogen Bonds Dictate the Coordination Geometry of Copper: Characterization of a Square-Planar Copper(I) Complex. *Angew. Chem.* **2016**, *128*, 3153–3157. [CrossRef]
34. Hussain, T.; Siddiqui, H.L.; Zia-Ur-Rehman, M.; Yasinzai, M.M.; Parvez, M. Anti-oxidant, anti-fungal and anti-leishmanial activities of novel 3-[4-(1H-imidazol-1-yl) phenyl] prop-2-en-1-ones. *Eur. J. Med. Chem.* **2009**, *44*, 4654–4660. [CrossRef] [PubMed]
35. Bauman, V.T.; Shults, E.E.; Kononchuk, V.V.; Bagryanskaya, I.Y.; Shakirov, M.M.; Tolstikov, G.A. Synthetic Transformations of Isoquinoline Alkaloids. 1-Alkynyl-3,6-dimethoxy-N-methyl-4,5α-epoxy-6,18-endoethenobenzo[i]isomorphinans and Their Transformations. *Russ. J. Org. Chem.* **2013**, *49*, 1502–1513. [CrossRef]
36. Cinčić, D.; Friščić, T.; Jones, W. Isostructural Materials Achieved by Using Structurally Equivalent Donors and Acceptors in Halogen-Bonded Cocrystals. *Chem. A Eur. J.* **2008**, *14*, 747–753. [CrossRef]
37. Turunen, L.; Beyeh, N.K.; Pan, F.; Valkonen, A.; Rissanen, K. Tetraiodoethynyl resorcinarene cavitands as multivalent halogen bond donors. *Chem. Commun.* **2014**, *50*, 15920–15923. [CrossRef]
38. Bock, H.; Holl, S. Wechselwirkungen in Molekülkristallen, 167 [1,2]. Kristallzüchtung und Strukturbestimmung von σ-Donator/Akzeptor-Komplexen zwischen 1,4-Dioxan und den Polyiod-Molekülen I_2,$I_2C{=}CI_2$, $(IC)_4S$ sowie $(IC)_4NR$ (R = H, CH_3)/Interaction in Molecular Crystals, 167 [1,2]. C rystallization and Structure Determination of σ-Donor/Acceptor Complexes between 1,4-Dioxane and the Polyiodine Molecules I_2,$I_2C{=}CI_2$, $(IC)_4S$ and (IC)4NR (R = H, CH_3). *Z. Für Naturforsch. B* **2001**, *56*, 111–121. [CrossRef]

39. Turunen, L.; Pan, F.; Beyeh, N.K.; Trant, J.F.; Ras, R.H.A.; Rissanen, K. Bamboo-like Chained Cavities and Other Halogen-Bonded Complexes from Tetrahaloethynyl Cavitands with Simple Ditopic Halogen Bond Acceptors. *Cryst. Growth Des.* **2017**, *18*, 513–520. [CrossRef]
40. Chu, Q.; Wang, Z.; Huang, Q.; Yan, C.; Zhu, S. Fluorine-containing donor-acceptor complexes: Crystallographic study of the interactions between electronegative atoms (N, O, S) and halogen atoms (I, Br). *New J. Chem.* **2003**, *27*, 1522. [CrossRef]
41. Roper, L.C.; Präsang, C.; Kozhevnikov, V.N.; Whitwood, A.C.; Karadakov, P.B.; Bruce, D. Experimental and Theoretical Study of Halogen-Bonded Complexes of DMAP with Di- and Triiodofluorobenzenes. A Complex with a Very Short N···I Halogen Bond. *Cryst. Growth Des.* **2010**, *10*, 3710–3720. [CrossRef]
42. Pearson, R.J.; Evans, K.M.; Slawin, A.M.Z.; Philp, D.; Westwood, N.J. Controlling the Outcome of an N-Alkylation Reaction by UsingN-Oxide Functional Groups. *J. Org. Chem.* **2005**, *70*, 5055–5061. [CrossRef] [PubMed]
43. Kroke, E.; Schwarz, M.; Horath-Bordon, E.; Kroll, P.; Noll, B.; Norman, A.D. Tri-s-triazine derivatives. Part I. From trichloro-tri-s-triazine to graphitic C_3N_4 structures. *New J. Chem.* **2002**, *26*, 508–512. [CrossRef]
44. Sun, W.; Zhu, G.; Wu, C.; Li, G.; Hong, L.; Wang, R. Organocatalytic Diastereo- and Enantioselective 1,3-Dipolar Cycloaddition of Azlactones and Methyleneindolinones. *Angew. Chemie Int. Ed.* **2013**, *52*, 8633–8637. [CrossRef] [PubMed]
45. Mustapha, A.; Reglinski, J.; Kennedy, A.R. The use of hydrogenated Schiff base ligands in the synthesis of multi-metallic compounds. *Inorg. Chim. Acta* **2009**, *362*, 1267–1274. [CrossRef]
46. Groom, C.; Bruno, I.J.; Lightfoot, M.; Ward, S.C. The Cambridge Structural Database. *Acta Crystallogr. Sect. B Struct. Sci. Cryst. Eng. Mater.* **2016**, *72*, 171–179. [CrossRef] [PubMed]
47. Sheldrick, G.M. SHELXT-Integrated space-group and crystal-structure determination. *Acta Crystallogr. Sect. A Found. Adv.* **2015**, *71*, 3–8. [CrossRef]
48. Bourhis, L.J.; Dolomanov, O.V.; Gildea, R.; Howard, J.A.K.; Puschmann, H. The anatomy of a comprehensive constrained, restrained refinement program for the modern computing environment *Olex2* dissected. *Acta Crystallogr. Sect. A Found. Adv.* **2015**, *71*, 59–75. [CrossRef]
49. Dolomanov, O.; Bourhis, L.J.; Gildea, R.; Howard, J.A.; Puschmann, H. OLEX2: A complete structure solution, refinement and analysis program. *J. Appl. Crystallogr.* **2009**, *42*, 339–341. [CrossRef]
50. Koziskova, J.; Hahn, F.; Richter, J.; Kozisek, J. Comparison of different absorption corrections on the model structure of tetrakis (μ2-acetato)-diaquadicopper(II). *Acta Chim. Slovaca.* **2016**, *9*, 136–140. [CrossRef]
51. Macrae, C.F.; Sovago, I.; Cottrell, S.J.; Galek, P.T.A.; McCabe, P.; Pidcock, E.; Platings, M.; Shields, G.P.; Stevens, J.S.; Towler, M.; et al. Mercury 4.0: From visualization to analysis, design and prediction. *J. Appl. Crystallogr.* **2020**, *53*, 226–235. [CrossRef]
52. Neese, F. Software update: The ORCA program system, version 4. *Wiley Interdiscip. Rev. Comput. Mol. Sci.* **2017**, *8*, e1327. [CrossRef]
53. Najibi, A.; Goerigk, L. The Nonlocal Kernel in van der Waals Density Functionals as an Additive Correction: An Extensive Analysis with Special Emphasis on the B97M-V and ωB97M-V Approaches. *J. Chem. Theory Comput.* **2018**, *14*, 5725–5738. [CrossRef] [PubMed]
54. Grimme, S.; Ehrlich, S.; Goerigk, L. Effect of the damping function in dispersion corrected density functional theory. *J. Comput. Chem.* **2011**, *32*, 1456–1465. [CrossRef]
55. Grimme, S.; Antony, J.; Ehrlich, S.; Krieg, H. A consistent and accurate ab initio parametrization of density functional dispersion correction (DFT-D) for the 94 elements H-Pu. *J. Chem. Phys.* **2010**, *132*, 154104. [CrossRef] [PubMed]
56. Noro, T.; Sekiya, M.; Koga, T. Segmented contracted basis sets for atoms H through Xe: Sapporo-(DK)-nZP sets (n = D, T, Q). *Theor. Chem. Acc.* **2012**, *131*, 131. [CrossRef]
57. Stoychev, G.L.; Auer, A.A.; Neese, F. Automatic Generation of Auxiliary Basis Sets. *J. Chem. Theory Comput.* **2017**, *13*, 554–562. [CrossRef] [PubMed]
58. Neese, F.; Wennmohs, F.; Hansen, A.; Becker, U. Efficient, approximate and parallel Hartree-Fock and hybrid DFT calculations. A "chain-of-spheres" algorithm for the Hartree-Fock exchange. *Chem. Phys.* **2009**, *356*, 98–109. [CrossRef]
59. Izsák, R.; Neese, F. An overlap fitted chain of spheres exchange method. *J. Chem. Phys.* **2011**, *135*, 144105. [CrossRef]

60. Lu, T.; Chen, F. Multiwfn: A multifunctional wavefunction analyzer. *J. Comput. Chem.* **2011**, *33*, 580–592. [CrossRef]
61. Lu, T.; Chen, F. Quantitative analysis of molecular surface based on improved Marching Tetrahedra algorithm. *J. Mol. Graph. Model.* **2012**, *38*, 314–323. [CrossRef]
62. Spackman, M.A.; McKinnon, J. Fingerprinting intermolecular interactions in molecular crystals. *CrystEngComm* **2002**, *4*, 378–392. [CrossRef]
63. Manna, P.; Seth, S.K.; Mitra, M.; Choudhury, S.R.; Bauzá, A.; Frontera, A.; Mukhopadhyay, S. Experimental and Computational Study of Counterintuitive ClO_4^- ... ClO_4^- Interactions and the Interplay between and Anion + Interactions. *Cryst. Growth Des.* **2014**, *14*, 5812–5821. [CrossRef]
64. Wolff, S.K.; Grimwood, D.J.; McKinnon, J.J.; Jayatilaka, D.; Spackman, M.A. *CrystalExplorer 3.1*; University of Western Australia: Perth, Australia, 2007.
65. Osborne, S.; Wellens, S.; Felton, S.; Gunaratne, H.Q.N.; Nockemann, P.; Ward, C.; Bowman, R.; Binnemans, K.; Swadzba-Kwasny, M. Thermochromism and switchable paramagnetism of cobalt(ii) in thiocyanate ionic liquids. *Dalton Trans.* **2015**, *44*, 11286–11289. [CrossRef] [PubMed]
66. Lomjanský, D.; Varga, F.; Rajnák, C.; Moncol, J.; Boča, R.; Titis, J. Redetermination of Zero-Field Splitting in $[Co(qu)_2Br_2]$ and $[Ni(PPh_3)_2Cl_2]$ Complexes. *Nova Biotechnol. Chim.* **2016**, *15*, 200–211. [CrossRef]
67. Manna, P.; Seth, S.K.; Mitra, M.; Das, A.; Singh, N.J.; Choudhury, S.R.; Kar, T.; Mukhopadhyay, S. A successive layer-by-layer assembly of supramolecular frameworks driven by a novel type of face-to-face π^+–π^+ interactions. *CrystEngComm* **2013**, *15*, 7879–7886. [CrossRef]
68. Mahmoudi, G.; Seth, S.; Zubkov, F.I.; Torres, E.S.L.; Bacchi, A.; Stilinović, V.; Frontera, A. Supramolecular Assemblies in Pb(II) Complexes with Hydrazido-Based Ligands. *Crystals* **2019**, *9*, 323. [CrossRef]
69. Johnson, E.R.; Keinan, S.; Mori-Sánchez, P.; Contreras-Garcia, J.; Cohen, A.; Yang, W. Revealing Noncovalent Interactions. *J. Am. Chem. Soc.* **2010**, *132*, 6498–6506. [CrossRef]
70. Humphrey, W.; Dalke, A.; Schulten, K. VMD: Visual molecular dynamics. *J. Mol. Graph.* **1996**, *14*, 33–38. [CrossRef]
71. Matta, C.F.; Boyd, R.J.; Becke, A. *The Quantum Theory of Atoms in Molecules: From Solid State to DNA and Drug Design*; Wiley-VCH: Weinheim, Germany, 2007.
72. Becke, A.D.; Edgecombe, K.E. A simple measure of electron localization in atomic and molecular systems. *J. Chem. Phys.* **1990**, *92*, 5397–5403. [CrossRef]
73. Lu, T.; Chen, F.W. Meaning and Functional Form of the Electron Localization Function. *Acta Phys. Chim. Sin.* **2011**, *27*, 2786–2792.